



Version 0.3

Measurement of $d\sigma(pp\bar{p} \rightarrow Z/\gamma^* \rightarrow e^+e^-)/dY$ at the Tevatron

The DØ Collaboration
(Dated: March 14, 2005)

We present the first Run II measurement of Z/γ^* decaying to e^+e^- inclusive differential cross section as a function of boson rapidity in the mass range between 71 to 111 GeV. The data were collected with the DØ detector at the Tevatron $p\bar{p}$ collider at $\sqrt{s}=1.96$ TeV. At Run II, Z bosons are produced with rapidities up to ± 3 . The cross section is measured over nearly the entire kinematic range.

Preliminary Results for Winter 2005 Conferences

I. INTRODUCTION

Precision electroweak measurements such as the W mass measurement at the Tevatron depend on the theoretical calculation of the W and Z boson cross-sections and their transverse momentum distributions. The precision of these quantities is currently limited by the uncertainties in the parton distribution functions (PDFs) which are used in the calculations.

The measurement of PDFs at high momentum transfer (Q^2) and high Bjorken x at hadron colliders has traditionally been performed using high-momentum jet spectra. An alternative tool for studying the PDFs is dilepton production. The Z /Drell-Yan process offers a complementary measurement with systematic errors almost wholly different than those in the standard analyses. The leptonic signature allows for precise measurement of the energies involved. There are significant theoretical advantages to the process as well; the Z /Drell-Yan process rapidity distributions can be calculated with NNLO precision [1].

In this note, we describe a measurement of the differential cross-section

$$\frac{1}{\sigma} \frac{d\sigma(p\bar{p} \rightarrow Z/\gamma^* \rightarrow e^+e^-)}{dY} = \frac{1}{\sigma} \frac{N_i^{obs} - N_i^{bkgd}}{\Delta_i(\epsilon \times A)_i \mathcal{L}}, \quad (1)$$

extracted in bins of Z -boson rapidity $Y = \frac{1}{2} \ln \frac{E^Z + p^Z}{E^Z - p^Z}$. At leading order, the rapidity of the Z is directly connected to the difference in Bjorken x parameters of the initiating quark and antiquark, so this measurement can provide information to constrain the parton distribution functions at $Q^2 \approx M_Z^2$.

The data used in this analysis was acquired by the $D\bar{O}$ experiment between August 2002 and June 2004. After removing bad luminosity blocks and bad runs, the luminosity for the trigger set described in Sec. II B 4 is 337 pb^{-1} .

II. ANALYSIS METHOD

A. Event Selection

The event selection requires two good EM objects, one with $p_T > 25 \text{ GeV}/c$ and a second with $p_T > 15 \text{ GeV}/c$. Both EM objects must pass cuts of Isolation < 0.15 and EM fraction > 0.9 . Electrons are considered to be in the Central Calorimeter (CC) if they have $|\eta_D| < 1.1$. These objects must be within the central 80% of a calorimeter ϕ -module. Electrons in the CC region are required to have a loose track match (EM ID = ± 11) and also have a tight spatial track match. In addition, CC region electrons must have an electron like shower shape (H-Matrix(7) < 12). Candidate electrons in the End Cap Calorimeters (EC) are used if they have $1.5 < |\eta_D| < 3.2$, EM ID = 10 or ± 11 , and satisfy shower shape requirements (H-Matrix(8) < 20). One of the candidate electrons must satisfy the trigger requirements (see Sec. II B 4) and at least one must have a tight spatial track match (see Sec. II B 2). Electron candidates are rejected if they fall within run-dependent (η_D, ϕ) bad calorimeter regions as defined by Reference [2]. The invariant mass of the electron pair is required to be between $71 < M_{ee} < 111 \text{ GeV}/c^2$.

B. Efficiency Measurements

The rapidity distribution determined from applying the event selection must be corrected for the efficiency and acceptance in the detector. As described in detail below, we calculate the efficiency \times acceptance using a Monte Carlo program and single-electron efficiencies. We determine these efficiencies from the data using tag and probe methods with Z bosons.

1. Preselection Efficiency

For the tag and probe method used in determining the preselection efficiency, the tag is a track-matched electron and the probe is an isolated track. The tag electron is required to pass all of the selection cuts given in Section II A with $p_T > 25 \text{ GeV}$. Additionally, it must be within $|\eta_D| < 2$. The probe track must have $p_T > 12 \text{ GeV}/c$. The track position, projected to the third floor of the EM calorimeter, must be in the fiducial region for EM objects. A track-isolation cut is applied at $p_T < 3 \text{ GeV}/c$ on the scalar sum of all tracks within a cone of $\Delta R < 0.4$ about the candidate track. Tracks which overlap with muons are not used. Cuts are made on the tag-probe pair: the two tracks must be back to back in ϕ , they must originate from the same vertex, and the mass of the tag-probe pair must be

greater than $65 \text{ GeV}/c^2$. Probe tracks are considered to have passed if they are close in space to an EM object with $ID = 10, \pm 11$, isolation < 0.15 , and EM fraction > 0.9 .

The number of events that pass and fail are determined via Eqs. 2 and 3 respectively.

$$P = N_{pass}^{os} + N_{pass}^{ss} - 2B_{pass} \quad (2)$$

$$F = \frac{N_{fail}^{os} - N_{fail}^{ss}}{(1 - 2P_{mm}^t)(1 - 2P_{mm}^p)} \quad (3)$$

N^{xx} is the number of probes when the charge of the probe track was opposite to (*os*) or the same as (*ss*) that of the tag electron. B_{pass} is the background which passes the preselection cuts and is assumed to be negligible. P_{mm}^t (P_{mm}^p) is the probability that the charge on the tag (probe) was mismeasured. P_{mm} is less than 1% at low values of η_D and increases up to $\approx 20\%$ at the largest values of η_D used. Background contributions to the preselection come from multi-jet events and W +jet events and are charge symmetric. The N_{fail} terms in Eq. 3 are dominated by background. Background is removed by taking the difference of these terms.

The efficiency is applied as a function of η_D of the electron. In the CC region, the data are further divided into low and high p_T bins. The effect of a residual background component in the preselection efficiency is estimated by taking 1% of the total background, adding it to the number of failed probes, and redetermining the efficiency. The change to the efficiency is taken as a correlated systematic uncertainty.

2. Track Matching Efficiencies

In the central calorimeter region, we require all electrons to have a loose track match. The efficiency for loose track matching is determined using a tag and probe method, where the tag electron is required to pass the normal electron requirements including a tight track match requirement. The probe electron must pass EM ID and H-Matrix requirements and must be in the central 64% of the calorimeter cell. The tag and probe electrons must have a dielectron mass within $\pm 11 \text{ GeV}/c^2$ of M_Z to reject background. The efficiency is the fraction of probe electrons having a loose track match and is determined as a function of the z -vertex of the event and the η_D of the electron. The loose track matching efficiency is fairly flat as a function of η_D and averages 97%. A correlated systematic uncertainty is determined by estimating the residual effect of background in the peak and is also shown in the figure.

The event selection requires at least one of the two electrons to have a tight spatial track match. As for the loose track match, a tag and probe method is used with the tag electron having the normal electron requirements and a tight track match. The probe electron must pass EM ID and H-Matrix requirements and electrons in the central calorimeter are required to have a loose track match. The tag and probe electrons must have a dielectron within $\pm 20 \text{ GeV}/c^2$ of M_Z to reject background. The efficiency is the fraction of probe electrons with a tight track match and is determined as a function of η_D and the z -vertex of the event. The central track matching efficiency averages 95%, while the efficiency drops for electrons in the end caps from 92% at $|\eta_D| = 1.5$ to 25% at $|\eta_D| = 3.0$.

3. H-Matrix Efficiencies

A standard tag and probe method is used to determine H-Matrix efficiency in this analysis. Tag electrons must pass the standard electron criteria, and the probe electrons must as well, with the exception of the H-Matrix cut. We subtract the background using a Breit-Wigner convoluted with Gaussian curve to fit the invariant mass peak and a background shape from the fake EM objects by requiring H-Matrix(7) > 25 in the CC region and H-Matrix(8) > 35 in the EC region.

For the final $\epsilon \times A$ calculation, we use a two dimensional p_T and η_D H-Matrix efficiency, applying different H-Matrix efficiencies on electrons with tight track match and without tight track match. The reason for this is that the H-Matrix distributions are different for probes with and without a tight track match, even when the dielectron mass is very close to the Z mass. The average H-Matrix efficiency in the EC is 95%, and the average efficiency for CC region electrons is 96%.

4. Trigger Efficiencies

The data used in this analysis were acquired under several different trigger lists beginning with trigger list v8 and continuing until the end of the v12 list. Runs were combined into three groups for the trigger analysis : runs using trigger lists v8-v10, runs using trigger list v11, and runs using trigger list v12. These divisions are motivated by

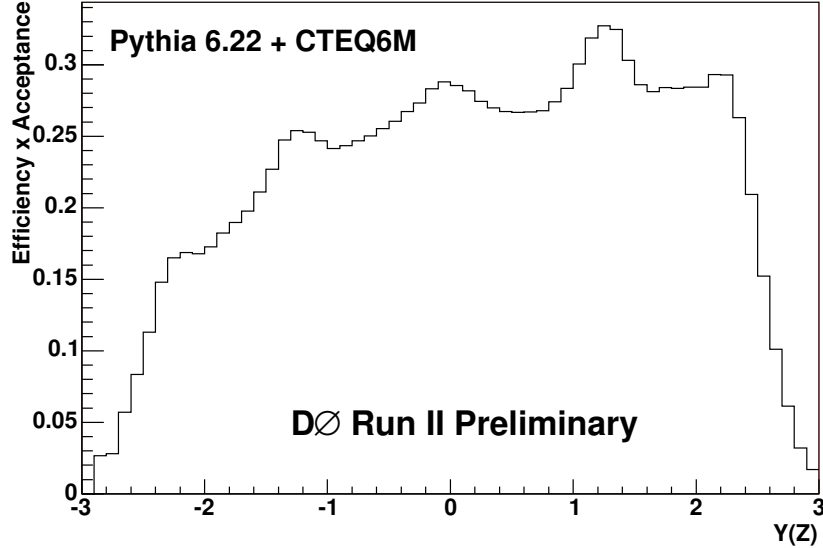


FIG. 1: Result of the $\epsilon \times A$ calculation. The asymmetry of the $\epsilon \times A$ distribution comes from the run-dependent calorimeter acceptance cuts, which primarily affect the negative endcap.

significant changes in the trigger hardware or trigger requirements. Trigger list v11 extended L1CAL coverage from $\eta = 2.4$ to $\eta = 3.2$, while the electromagnetic portion of the trigger list was greatly altered from v11 to v12.

Nine triggers are used for the analysis. For trigger lists v8-11 the triggers are EM_HI_SH, HI_2EM5_SH, EM_HI, EM_MX_SH, and EM_MX. For trigger list v12 the triggers used are E1_SHT20, E2_SHT20, E3_SHT20, and E1_SH30. Only unrescaled triggers are used. For the current data set, a trigger's prescale is set for the run duration. A decision list is used to select the combination of triggers per run.

The trigger efficiencies were determined using a tag and probe method. The tag electron, besides passing the normal electron requirements and having a tight track match, is required to pass a trigger. To pass a trigger, an electron must satisfy Level-1, Level-2, and Level-3 requirements. The probe electron need not have a tight track match. The trigger efficiency is the fraction of probe electrons which pass a trigger. The efficiencies were found to be dependent on the p_T and the η_D of the electrons.

C. Efficiency*Acceptance Calculation

The individual electron efficiencies, which are determined as functions of detector space and run, must be combined to determine the total efficiency as a function of Z -boson rapidity.

$$\begin{aligned}
 \epsilon_Z = & \epsilon_{\text{pre}}(\eta_{D1}, p_{T1}, v_z) * \epsilon_{\text{pre}}(\eta_{D2}, p_{T2}, v_z) * \\
 & \epsilon_{\text{lt}}(\eta_{D1}, v_z) * \epsilon_{\text{lt}}(\eta_{D2}, v_z) * \\
 & \epsilon_{\text{hmx}}(\eta_{D1}, p_{T1}, \text{track}_1) * \epsilon_{\text{hmx}}(\eta_{D2}, p_{T2}, \text{track}_2) * \\
 & [1 - (1 - \epsilon_{\text{tt}}(\eta_{D1}, v_z)) * (1 - \epsilon_{\text{tt}}(\eta_{D2}, v_z))] * \\
 & [1 - (1 - \epsilon_{\text{trig}}(\eta_{D1}, p_{T1}, \text{run})) * (1 - \epsilon_{\text{trig}}(\eta_{D2}, p_{T2}, \text{run}))]
 \end{aligned} \tag{4}$$

The $\epsilon \times A$ for each bin of rapidity is determined by applying the measured electron identification, trigger, and track matching efficiencies to Monte Carlo events generated by Pythia 6.220 and smeared using the D0 fast simulation package, Parameterized Monte Carlo Simulation (PMCS). The same acceptance cuts applied to the data are applied to the Monte Carlo and random trials are used to determine if a given event passes or fails the efficiency cuts. In the case of the H-Matrix efficiency, the trial on tight track matching is performed first and then the appropriate H-Matrix efficiency (track or no track) is used. A sample of 8.6M Monte Carlo events is used to determine the $\epsilon \times A$. The final $\epsilon \times A$ is shown in Fig. 1.

D. Data and Monte Carlo Comparison

Data and Monte Carlo distributions are compared to cross check the acceptance determination. These are shown in Fig. 2. All Monte Carlo distributions are scaled by the ratio of the number of events in the Z peak in Fig. 2(d). No background subtraction has been performed on the data presented in these plots. All errors presented in these plots are statistical. The plots generally agree well.

III. SYSTEMATIC UNCERTAINTIES

The systematic uncertainties in this measurement arise from the individual efficiencies used in the $\epsilon \times A$ calculation as well as from uncertainties and potential miscalibrations in the Monte Carlo used for the calculation. The effect of each of these uncertainties is propagated to the $\epsilon \times A$ curve. An additional systematic uncertainty enters with the background subtraction, which is described in Sec. IV.

For the efficiencies, both statistical (random) and correlated systematic effects are considered. The magnitude of a correlated systematic shift is evaluated as part of the measurement of each efficiency, and the size of these correlated uncertainties are shown individually with each efficiency. The $\epsilon \times A$ is recalculated using the shifted efficiencies; the variation of the $\epsilon \times A$ is considered to be the propagated error, which is plotted as a fractional error in Fig. 3(a) for each efficiency separately.

The statistical uncertainties from the limited numbers of events available for efficiency determination are also propagated through the $\epsilon \times A$ calculation. Each bin of each efficiency is shifted randomly based on the predicted distribution of efficiencies and the $\epsilon \times A$ is recalculated for the new efficiencies. This process is repeated multiple times to determine the effect of the statistical uncertainty on the efficiencies. For all efficiencies except the preselection efficiency, the efficiency is defined by a numerator n and denominator d number of events which form a binomial distribution. Accordingly, we use the binomial probability function [3]

$$P(\epsilon) = \frac{(d+1)!}{n!(d-n)!} \epsilon^n (1-\epsilon)^{d-n} \quad (5)$$

for these efficiencies. As described above, the preselection efficiency is determined in a slightly different manner, so random trials on that efficiency are determined by individual trials on the components of the efficiency. With some algebra, the efficiency derived from Eq. 2 and Eq. 3 can be written as

$$\frac{1}{\epsilon_i} = 1 + \frac{(\tilde{P}(N_{fail}^{ss}) + \tilde{P}(N_{fail}^{os} - N_{fail}^{ss}) - \tilde{P}(N_{fail}^{ss})) * \tilde{G}(f_q, \sigma_q)}{\tilde{G}(P, \sqrt{P})} \quad (6)$$

where $\tilde{P}(N_{fail}^{os} - N_{fail}^{ss})$ is a Poisson random number with mean value equal to the estimated number of failed signal events, $\tilde{P}(N_{fail}^{ss})$ are independent Poisson random numbers with mean value equal to the number of failed same-sign events, $\tilde{G}(f_q, \sigma_q)$ is a Gaussian random trial on the charge mis-id factor, and $\tilde{G}(P, \sqrt{P})$ is a Gaussian random trial on the number of events which pass preselection. The result of three hundred sets of trials was used to determine the statistical efficiency error in Fig 3(a).

Besides the uncertainties associated directly with the efficiencies, several uncertainties related to the Monte Carlo used for the $\epsilon \times A$ calculation are also calculated. These uncertainties include the parton density functions (PDFs) used by the Monte Carlo and the electromagnetic energy scale differences between data and the Monte Carlo. The boson p_T distributions used by the Monte Carlo also are taken into account as is the vertex distribution along the beam axis.

The $\epsilon \times A$ calculation uses Pythia with the CTEQ6M PDFs as input to apply the single-electron efficiencies. Variation of the PDFs could affect the acceptance of the analysis, and this variation is taken into account using the uncertainties provided with the CTEQ6 PDFs. The CTEQ6 PDFs are defined by twenty parameters, which are shifted separately to their positive and negative 1σ limits, providing a set of forty PDFs for error determination. We generated 5.6M events for each of the forty PDFs and performed the $\epsilon \times A$ calculation with each variation to determine the shift in the $\epsilon \times A$. The result is shown in Fig. 3(b).

Systematic mismeasurement of electron energies will affect both the calculation of the rapidity and the $\epsilon \times A$ calculation for any efficiency which depends on the electron energy (p_T). To evaluate the effect of energy scale uncertainties on the analysis, we determine the change in the $\epsilon \times A$ after scaling the energies of the electrons separately in each portion of the calorimeter. This is estimated by comparing the Z peaks obtained with electrons both in the same portion with Z peaks from electrons split across two calorimeters. For the negative endcap, the scale factor

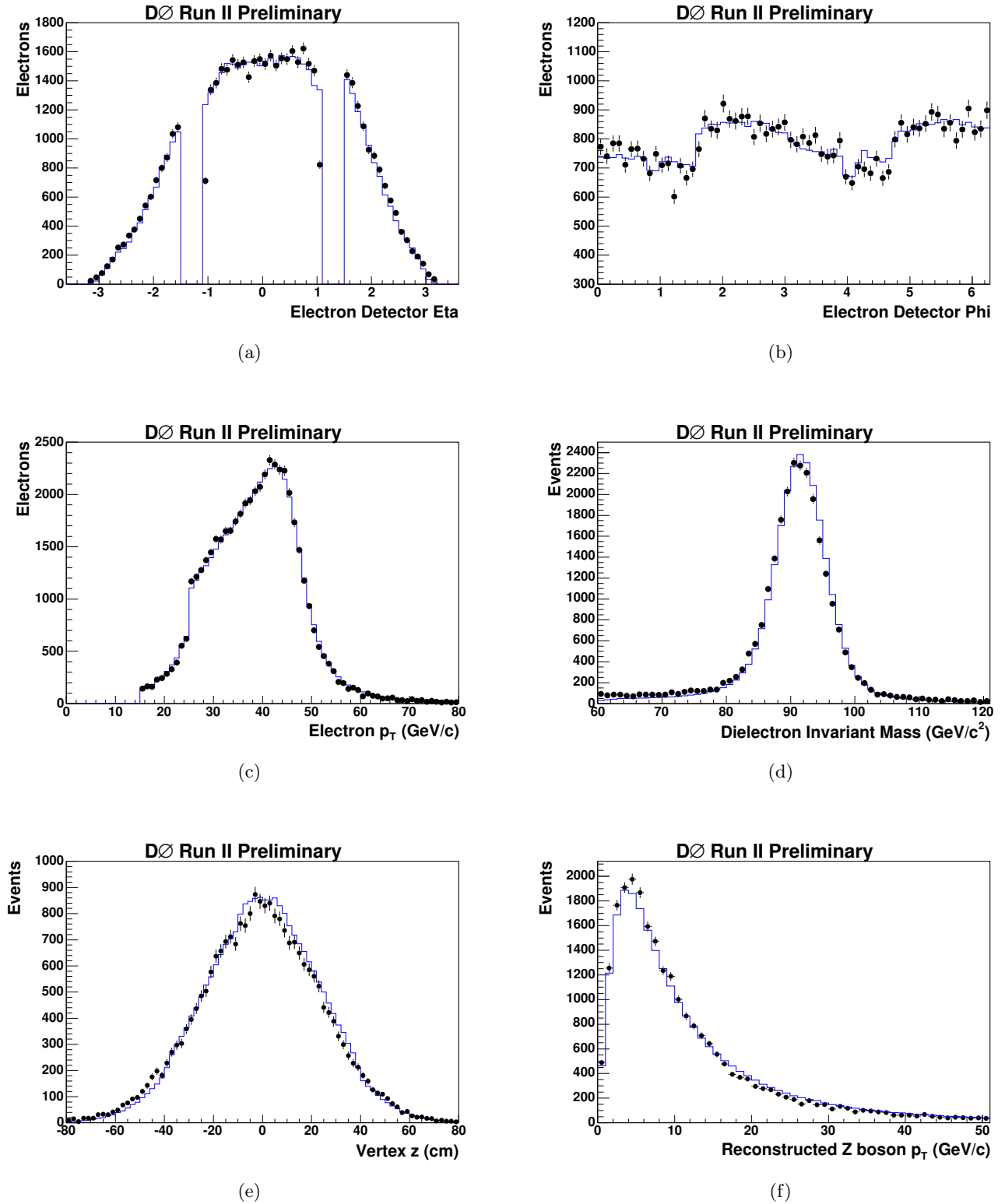


FIG. 2: Comparison between data and Monte Carlo for various electron and dielectron quantities. In each plot, the prediction of the Monte Carlo after the $\epsilon \times A$ calculation is shown as a dashed line and the data is shown as points.

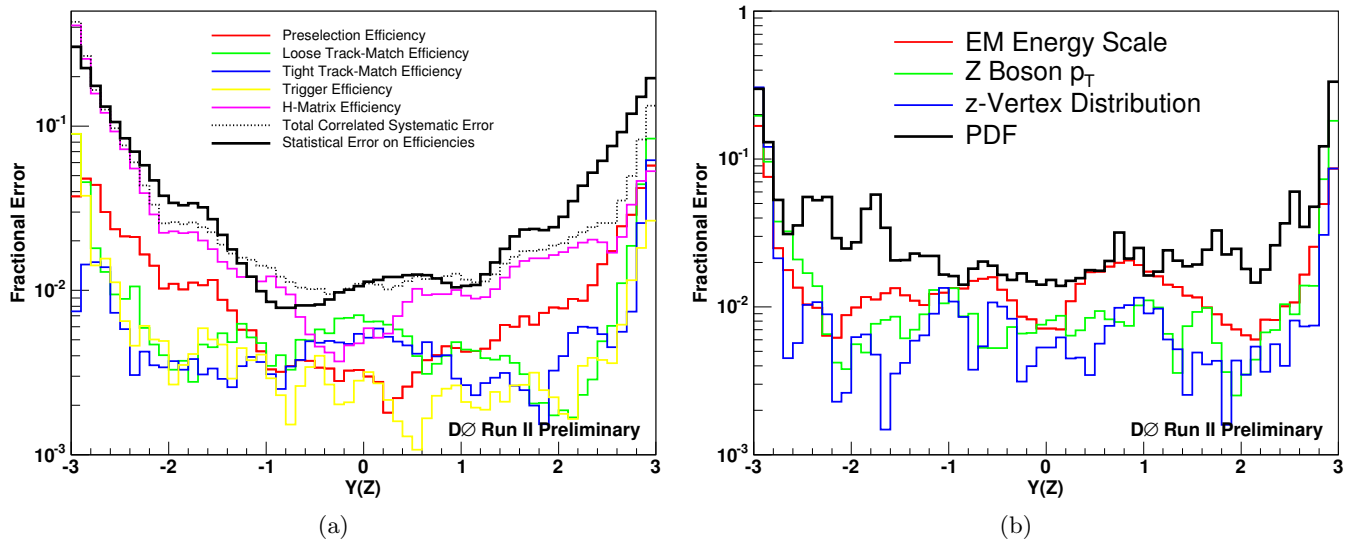


FIG. 3: Individual contributions to the systematic errors on the $\epsilon \times A$ calculation as a function of the boson rapidity. Errors derived from the efficiencies are shown in (a). The dotted line shows the combined error from correlated shifts in the efficiencies and the solid black line shows the combined error from the statistical uncertainties of the efficiencies. In (b) are fractional systematic errors from the PDFs, boson p_T , vertex z position, and calorimeter EM energy scale.

was 1 ± 0.0073 , for the positive endcap 1 ± 0.0046 , and for the central calorimeter 1 ± 0.0053 . The result is shown in Fig. 3(b).

The transverse momentum of the Z boson can have a significant effect on the final result by shifting the energies of the electrons for a given rapidity. Changing the energies of the electrons could sample different portions of the efficiency, leading to a systematic error. As part of tuning PMCS for this analysis, we developed a fit to the Z boson p_T parameters in Pythia. These parameters, shown in Table I, are slightly different than the ‘‘CDF Tune’’ [4] or ‘‘DØ tune’’ [5] given in the table. To evaluate the effect of shifting the Z boson p_T , we generated 6M events with the DØ and CDF tunes and compared the shape and $\epsilon \times A$ results with the base set. The result is shown in Fig. 3(b).

	Analysis Tune	CDF Tune	DØ Tune	Pythia Default
PARP(62)	1.0	1.25	1.0	1.0
PARP(64)	0.2	0.2	0.2	1.0
PARP(91)	1.5	2.5	1.3	1.0
PARP(93)	8.0	15.0	5.0	5.0

TABLE I: Pythia parameters related to the Z boson p_T . The tune used in this analysis, a tune from CDF, and a tune from DØ are shown.

Finally, the z vertex distribution used by PMCS was evaluated originally from a Higgs analysis looking at associated Z production in only a portion of the Pass 2 data set. It is possible that this distribution is biased in some way. To check, we created a z vertex distribution from the analysis but vetoed all electrons which were in the ϕ_D regions cut out by the bad calorimeter cuts, regardless of η_D . This was done to reduce the selection bias from the bad calorimeter regions. The original distribution and the distribution from the Z rapidity analysis are shown in Fig. 2 (e), and the effect is propagated as a systematic error as shown in Fig. 3(b).

In Fig. 4, the various contributions to the systematic error are summarized. While the PDF error is the single largest source of uncertainty, the combined errors from the single electron efficiencies dominate the error at large values of boson rapidity. For comparison, the statistical error also is shown.

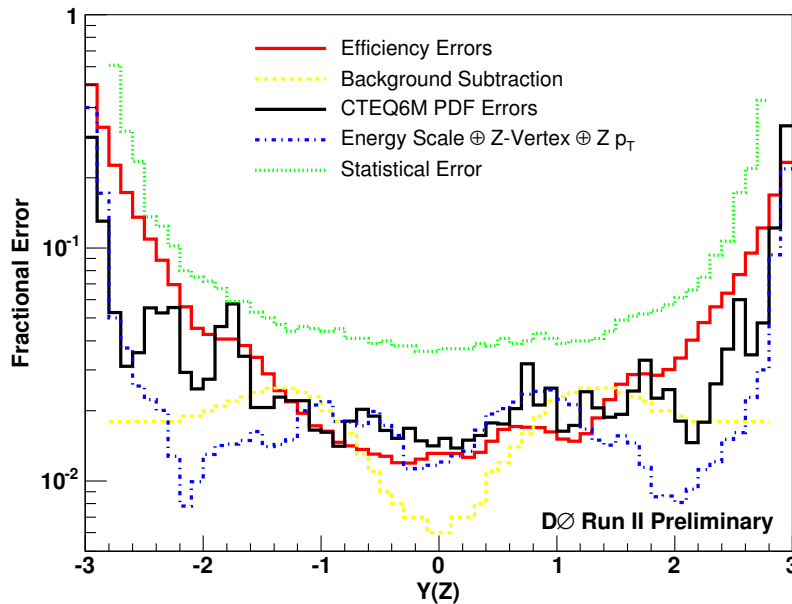


FIG. 4: Fractional errors as a function of boson rapidity.

Region	Fraction (%)
CCCC	1.55
CCEC	6.66
ECEC	4.91
All	5.20

TABLE II: Background fractions for events collected in different calorimeter regions. Fraction for all regions combined is measured separately and is shown for comparison.

IV. BACKGROUND

The main sources of background come from multijet events where two jets pass the selection cuts and from W +jet events where the jet is misidentified as an electron. To remove these backgrounds, fits are performed on the mass distributions of the data.

Background shapes are taken from data. To select background events, most of the selection cuts are applied. The track requirement is omitted and the H-Matrix value for each EM object must be greater than 30. Since the background shape is not expected to be the same for CC and EC regions, three shapes are acquired. One for CCCC events, one for CCEC events, and one for ECEC events.

A signal shape is obtained from $Z/\gamma^* \rightarrow ee$ Monte Carlo that has been processed with the DØ full simulation code. The Monte Carlo has been resmeared to better match the data. Monte Carlo events are binned in the same manner as the data.

The data are divided into three groups based on the three calorimeter combinations (CCCC, CCEC, and ECEC). A two parameter fit is made to the data. One parameter is the amplitude of the background shape and the other parameter is the amplitude of the signal shape. The scaled background shape is integrated in the mass region to determine the number of background events and the background fraction for a given calorimeter region. The background fraction is assumed to be constant within each calorimeter region. The background fraction for each combination is given in Table II. A systematic error is estimated by varying the fit range. For the final result, a 35% error is assumed on the background which is subtracted from each bin.

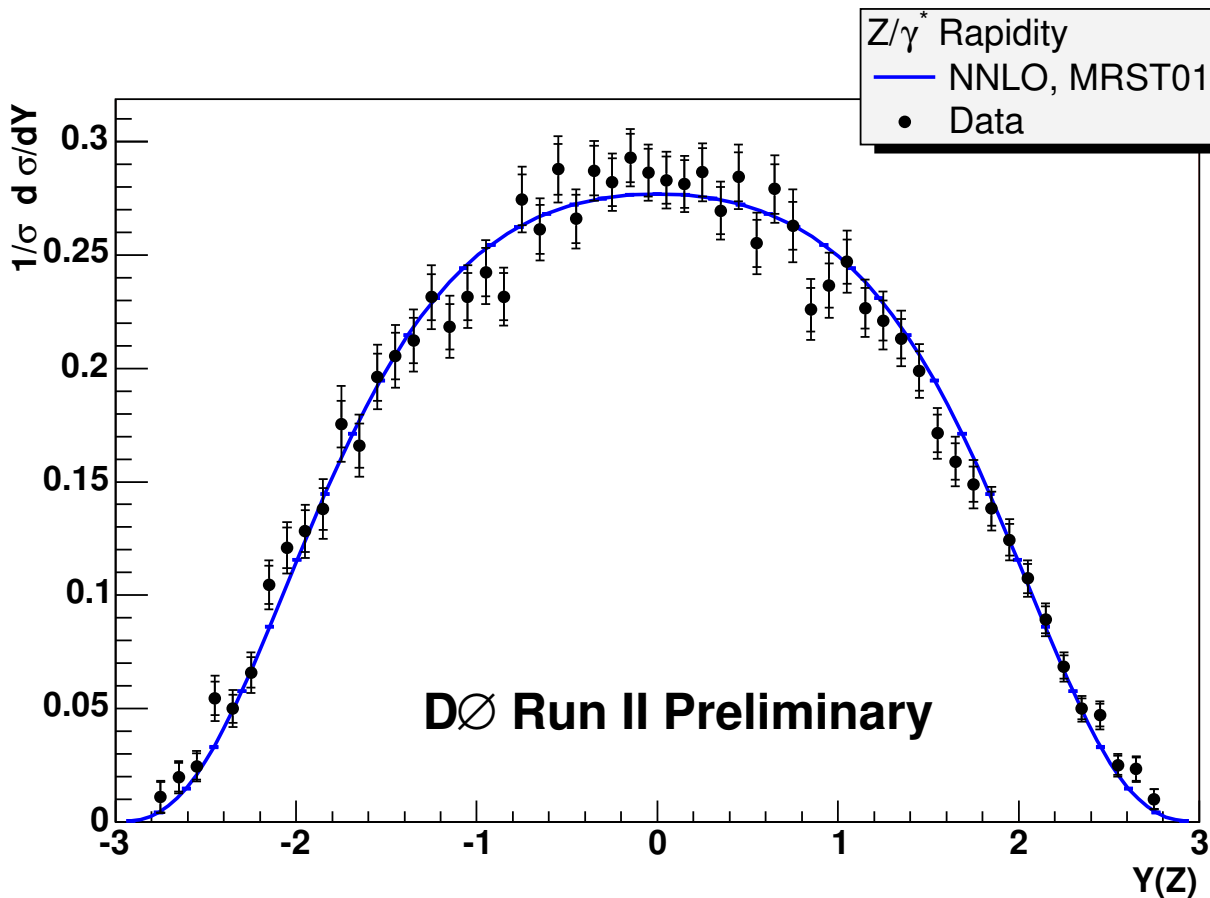


FIG. 5: Analysis result. The outer error bars show the total error, combining statistical and systematic errors, while the inner error bars indicate the statistical error alone. The solid line shows the NNLO prediction based on the MRST 2001 PDFs.

V. RESULT

For the final result, the systematic errors and the background subtraction errors are propagated through the defining equation

$$\begin{aligned}
 \frac{1}{\sigma} \frac{d\sigma(Z/\gamma^* \rightarrow e^+e^-)}{dY} &= \frac{1}{\sigma} \frac{N_i^{obs} - N_i^{bkgd}}{\Delta_i(\epsilon \times A)_i \mathcal{L}} \\
 &= \frac{1}{\sum_j \frac{N_j^{obs} - N_j^{bkgd}}{\Delta_j(\epsilon \times A)_j}} \frac{N_i^{obs} - N_i^{bkgd}}{\Delta_i(\epsilon \times A)_i} \quad (7)
 \end{aligned}$$

The final result with statistical and systematic errors, is shown in Fig. 5. The use of the DØ forward calorimeters provides data over almost the entire rapidity range accessible at the Tevatron. Fig. 5 also shows a prediction for the rapidity distribution for $Z/\gamma^* \rightarrow ee$ using an NNLO prediction based on the MRST 2001 parton density functions [1]. The data are in generally good agreement with the prediction.

-
- [1] C. Anastasiou, L. Dixon, K. Melnikov and F. Petriello, “High-precision QCD at hadron colliders: Electroweak gauge boson rapidity distributions at NNLO,” Phys. Rev. D **69**, 094008 (2004) [arXiv:hep-ph/0312266].
 [2] D.Chapin, *et. al.*, “Measurement of $Z \rightarrow ee$ and $W \rightarrow e\nu$ Production Cross Sections with $|\eta| < 2.3$ ”, DØ Note 4403, March 2003.

- [3] G. D'Agostini, "Bayesian reasoning in high-energy physics : principles and applications", CERN 99-03.
- [4] U. Yang and Y. Kim, "ISR Studies on Drell-Yan", Fermilab MC Workshop (2003), <http://cepa.fnal.gov/patriot/mc4run2/MCTuning/031204/unki.pdf>.
- [5] B. Tiller and T. Nunnemann, "Measurement of the Differential Z0-Boson Production Cross-Section as Function of Transverse Momentum", DØ Note 4660, December 2004.